Novel Research in Microbiology Journal (2023), 7(6): 2248-2264
Research Article

(Print) (ISSN 2537-0286)
(Online) (ISSN 2537-0294)
https://nrmj.journals.ekb.eg/
DOI: 10.21608/nrmj.2023.330426

The antibiofilm activity of purified and characterized mannan from *Saccharomyces cerevisiae* against multidrug-resistant *Escherichia coli*

Naam Fadhil Abbas Al-Helli*; Jehan Abdul Sattar Salman

Department of Biology, College of Science, Mustansiriyah University, Baghdad, Iraq

*Corresponding author E-mail: mscnh23@uomustansiriyah.edu.iq

Received: 17 November, 2023; Accepted: 13 December, 2023; Published online: 14 December, 2023

Abstract

Biofilm formation by *Escherichia coli* presents a major challenge in the clinical settings, resulting in persistent infections and treatment failures. These bacterial communities, protected by a matrix, resist antibiotics and immune responses, thus causing a prolonged challenge to treat such infections. Developing effective strategies against *E. coli* biofilms is crucial for improving the patient outcomes and reducing the burden on the healthcare systems. This study aimed to extract, purify, and characterize mannan from *Saccharomyces cerevisiae*, then its antibiofilm activity was evaluated against the multi-drug resistant *E. coli* (MDR-*E. coli*) isolates obtained from various clinical sources (*i.e.*, urine, stool, wound, and catheter). Using a standardized protocol with slight modifications, the crude mannan extraction yielded 37.6 %, and subsequent purification achieved an efficiency of 99.6 %. Characterization assays of the purified mannan included FT-IR; FE-SEM, carbohydrate content estimation, solubility, and melting point tests, which revealed the presence of α-1,6 and α-1,2 linked sugars; crystalline nature, high porosity (80 %) carbohydrate content, high solubility in water, and a melting point of 248 °C. The purified mannan exhibited a substantial ability to inhibit biofilm formation (37.50 %) and degrade the existing MDR-*E. coli* biofilms (37.43 %). These findings underscore the potential of *S. cerevisiae* mannan as an effective antibiofilm agent for the clinical applications. Further exploration and optimization of the mannan's therapeutic potential are essential to fully leverage its efficacy in combating the biofilm-associated infections caused by MDR-*E. coli*.

Keywords: Biofilm inhibition, Mannan, Baker's yeast, FE-SEM, FT-IR, Antibacterial activity

1. Introduction

Bacterial infections, which are ranked as the second leading cause of death in the developing nations, are influenced by several factors, such as immune status, age, and antibiotic resistance (Salam *et al.*, 2023). *Escherichia coli* (*E. coli*) is a critical concern bacterial pathogen, due to its involvement in

fatal infections, including bloodstream infections and pneumonia. According to Sonola *et al*., (2022), the World Health Organization (WHO) recognized this antibiotic-resistant bacterium as a primary culprit in the prevalence of hospital-acquired diseases and urinary tract infections (UTI). Multidrug-resistant *E. coli* (MDR-*E. coli*) refers to strains of this bacterium that have developed resistance to multiple antibiotics, which poses a challenge in treating infections caused by these strains. Mechanisms contributing to this antibiotic resistance include efflux pumps; antibiotic modification, target site changes, and plasmid-mediated resistance (Tong *et al*., 2023). MDR-*E. coli* is a significant public health concern worldwide due to its common presence and the difficulty to treat its infections. Addressing this issue involves responsible antibiotic use, surveillance, and infection control measures. Compounding this issue is the bacterium's capacity to create a biofilm on both of the living and inanimate surfaces (Elsayed *et al*., 2023). Biofilm-associated infections present a formidable clinical challenge, which are characterized by persistent infections; heightened antibiotic resistance, and compromised patient outcomes (Haney and Hancock, 2022). The National Health Guidelines attributed 80 % of all the human body infections to biofilms (Ballén *et al*., 2022), which are structured microbial communities encased in a protective matrix of extracellular polymeric substances (EPS) (Laconi *et al*., 2023). This matrix shields the microorganisms from antibiotics; the immune system, and the other external threats; making biofilm-associated infections more resistant to treatment compared with infections caused by the free-floating microorganisms. Innovative approaches are urgently needed to address these biofilm-related infections effectively. The cell wall of *Saccharomyces cerevisiae* (*S. cerevisiae*) consists predominantly of polysaccharides; constituting approximately 90 % of the components and accounting for 15-25 % of the dry weight of the yeast cell (Yousefi, 2023). The existing polysaccharides include mainly β-glucans (55-65 %); mannoprotein (35-40 %), glycogen (1-29 %), and chitin (1-2 %) (Reis *et al*., 2023). Mannan is a complex polysaccharide composed of mannose residues linked by α-1,6 bonds with branching at α-1,2 and α-1,3 positions, which expresses diverse biological properties and potential applications (Gil *et al*., 2023). *S. cerevisiae* has emerged as a promising source of mannan, thus it is extensively used in the biotechnological processes. Moreover, *S. cerevisiae* is known for its affordability and sustainable production methods (Abdulhameed *et al*., 2020). Understanding the cost-effectiveness of *S. cerevisiae*-derived mannan could lead to accessible and innovative solutions, and offering new avenues for combating the biofilm-associated infections in the clinical practice. The objectives of this study were to focus on the extraction; purification, and characterization of mannan obtained from *S. cerevisiae*, and to gain insights into its therapeutic potential in combating the biofilm-associated infections caused by MDR-*E. coli*.

2. Materials and methods

2.1. Microorganisms

Five different types of compressed commercial Baker's yeast (*S. cerevisiae*) were purchased from Iraqi local markets. They were identified through a comprehensive approach involving cultural methods; microscopic examination, and the VITEK®2 system (BioMérieux). Meanwhile, a total of 112 isolates of *E. coli* were isolated from various clinical samples, including urine; catheters, wounds, and stools, collected from patients of both sexes admitted to several Iraqi hospitals (*i.e*., Ibn Al-Nafis; Sheikh Zayed, and Al-Alawi Maternity). These isolates were identified through cultural methods, microscopic examination, and biochemical assays following the guidelines outlined in Bergey's Manual of Determinative Bacteriology (Brenner *et al*., 2005), in addition to the VITEK®2 system (BioMérieux). All the identified *E. coli* isolates were investigated for their antimicrobial susceptibility test (AST) following CLSI guidelines. The used testing was Kirby Bauer's disk diffusion method that included nine commonly prescribed antibiotics; mainly Amikacin (30 µg), Gentamicin (10 µg), Cefotaxime (30 µg), Ceftriaxone (30 µg), Ciprofloxacin (5 µg), Norfloxacin (10 µg),

Trimethoprim-Sulfamethoxazole (1.25/ 23.75 µg), Tetracycline (30 µg), and Imipenem (10 µg). The microorganisms that showed resistance to at least three antibiotics from the diverse classes were classified as multidrug-resistant (MDR), according to the criteria established by Kunz Coyne *et al*., (2022). Moreover, the biofilm formation assay was carried out to select the MDR and biofilm forming isolates. The microtiter plate method conducted by Ballash *et al*., (2022) was used, involving a 96-well microplate that was filled with Brain Heart Infusion (BHI) broth and 2 % sucrose. After inoculation; incubation, washing, and staining with crystal violet, the optical density (OD) readings were measured at 630 nm and then categorized, allowing for evaluation of the biofilm formation potential among the tested *E. coli* isolates.

2.2. Mannan extraction

Mannan was extracted from the Baker's yeast samples following the method described by Huang *et al*., (2010) with slight modifications. Five gram portion of the dried yeast was added to 50 ml of 1 % NaOH and heated at 100 °C for 2 h, and the resulting solution was neutralized to pH 7 using HCl (10 %). Subsequently, the mixture had undergone a gravity filtration using a Whatman filter paper (47 mm) with a pore size of 0.7 µm. To the sediment, 200 ml of 96 % ethanol was added, followed by centrifugation at 4000 rpm for 15 min. The sediment was washed with absolute ethanol, thoroughly mixed using a vortex mixer, and then centrifuged again at 4000 rpm for 15 min. The filtrate was discarded, while the sediment was washed with diethyl ether, mixed by vortex, and subjected to centrifugation at 4000 rpm for 15 min. The resulting precipitate was dissolved in an appropriate quantity of dist. H_2O to obtain a crude mannan.

2.3. Estimation of the mannan yield

To identify *S. cerevisiae* isolates with the highest crude mannan yield for the deproteinization process, a selection process was conducted using Equation (1) of Al-Manhel and Niamah, (2017):

$$\text{Mannan yield} = (\text{dry wt.}/\text{total wt.}) \times 100 \quad (1)$$

Where; dry wt.: is the dry weight of crude mannan, and total wt.: is the *S. cerevisiae* sample weight (5 g). The protein content (concentration) of crude mannan was measured using a UV absorbance-based method, referring to Equation (2) that was reported by Zhao *et al*., (2022):

$$C = 1.45 \times A_{280} - 0.74 \times A_{260} \quad (2)$$

Where; (C): represents the protein concentration of mannan (mg/ ml), and (A_{280} nm) and (A_{260} nm) represent the respective absorbance wavelengths of the crude mannan.

2.4. De-proteinization of mannan

The crude mannan extracted from the highest yielding yeast isolate was subjected to deproteinization following the method described by Huang, (2008) with minor modifications. The crude mannan was treated with 10 % trichloroacetic acid (TCA) until the pH reached 3. The mixture was then kept at 4 °C for 24 h and subsequently centrifuged at 4000 rpm for 15 min. The filtrate was precipitated by adding 3 volumes of 96 % ethanol and left at 4 °C for 24 h. The sediment obtained after centrifugation at 4000 rpm for 15 min. was dissolved in dist. H_2O and then heated in a hot water bath at 121°C for 3 h. Two replicates were used to ensure the validity of the results.

2.5. Characterization of mannan

1. Fourier transform infrared spectrometer (FT-IR)

The FT-IR instrument (Bruker Corporation, ALPHA II, USA) was used to analyze the organic groups present in mannan. FT-IR analysis was conducted across a wavelength range of 400-4000 cm^{-1}; enabling a detailed examination of molecular vibrations of the functional groups, in addition to the distinctive features within the mannan powder (Cerqueira *et al*., 2011). Two replicates were used in this assay.

2. Field emission scanning electron microscopy (FE-SEM)

The FE-SEM (FEITM, Inspect-F50, Netherland) was employed as a powerful imaging technique to examine the morphology; microstructure, surface characteristics, particle size, and shape of mannan. Each assay was conducted using two replicates.

3. Phenol sulfuric acid method for carbohydrates content estimation

The Colorimetric method described by DuBois *et al*., (1956) was adopted, utilizing mannose as a standard carbohydrate. A reference solution of mannan (0.1 mg/ 100 ml dist. H_2O) was prepared and further diluted to obtain various concentrations, involving 0.2; 0.4, 0.6, 0.8, 1 ml). Afterwards, 0.1 ml and 0.2 ml of the mannan sample were transferred into two separate tubes; respectively, and the volume was adjusted to 1 ml using dist. H_2O. Approximately, 1 ml of 5 % phenol and 5 ml of 96 % sulfuric acid were added. The absorbance was measured at 490 nm using an Optima™ spectrophotometer (Japan). Two replicates were used.

4. Solubility assay

The solubility test of mannan was examined according to the protocol outlined in the European Pharmacopoeia (Zimmer *et al*., 2022). Approximately 1 g sample of ground mannan was mixed with increasing volumes of dist. H_2O, and its solubility classification was determined based on the volume of H_2O required for its complete solubilization. The mannan samples that dissolved in 10-30 ml; 30-100 ml, 100-1000 ml, and 1000-10000 ml of H_2O were classified as soluble; sparingly soluble, slightly soluble, and very slightly soluble, respectively. Two replicates were used.

5. Melting point

Using the STUART SMP30 Melting point Apparatus (UK), a suitable quantity of the purified mannan was filled into a closed-end capillary tube. The tube was then loaded into the melting point apparatus, and the melting point of mannan was measured following the protocol described by Dash *et al*., (2023). Two replicates were used.

2.6. Antibacterial potential of mannan against MDR-*E. coli* isolates

The antibacterial activity of mannan obtained from *S. cerevisiae* was evaluated using the micro dilution method of Loo *et al*., (2018), in order to determine its Minimum inhibitory concentration (MIC). This was replicated two times to ensure validity of the results. Dilute concentrations of mannan ranging from 3.125 to 200 mg/ ml were prepared. Approximately 125 µl of MH broth was added aseptically to each well of the 96 wells microplate. Subsequently, 125 µl of mannan (200 mg/ ml) was added to the first column and mixed with the medium. Then, 125 µl was serially transferred to the subsequent wells, while 125 µL of the mixture in the last column was discarded; so that the final volume in each well became 125 µl. Bacterial suspension (0.5 MacFarland) of each *E. coli* isolate was prepared individually using physiological saline and then diluted to 1:100 with MH broth. All wells were inoculated individually with 25 µl of each diluted bacterial suspension. The microtiter plate was then covered and incubated for 24 h at 37 °C. After incubation, 30 µl of Resazurin dye (0.015 %) was added to each well, and any color change from dark blue to bright pink was observed indicating dye reduction. The MIC was identified as the lowest concentration of mannan that prevented bacterial growth, signified by no reduction of the dye and no color change. It's noteworthy that one negative control column was used that contained MH broth only, while the positive control column included MH inoculated with the bacterial suspension.

2.7. Antibiofilm activity of mannan against MDR-*E. coli*

To estimate the inhibitory potential of mannan on biofilm formation by MDR-*E. coli*, a crystal violet assay was employed, according to the method

conducted by Haney *et al*., (2021) with slight modifications. By using a 96-well flat-bottom plate, the control well was filled with 200 µl of dist. H_2O, while the remaining wells were treated with 200 µl of sub-MIC of mannan, and then the plate was incubated at 37 °C for 24 h. Next, contents of the wells were discarded, washed with dist. H_2O, and allowed to dry at room temperature. Afterwards, 200 µl of the bacterial suspension (0.5 MacFarland) was added individually to the wells, and the plate was incubated at 37 °C for 24 h. The wells were then stained with 200 µl of 0.1 % crystal violet for 20 min., rinsed three times with dist. H_2O, and left to dry. Finally, 200 µl of 95 % ethanol was added to all wells, and the absorbance of the wells was measured at a wavelength of 630 nm using an ELISA reader. Two replicates were used. The percentage (%) of inhibition of biofilm formation by *E. coli* was determined using Equation (3) of Topa *et al*., (2018):

$$\text{Biofilm formation inhibition (\%)} = ((OD_C - OD_T)/OD_C) \times 100 \quad (3)$$

Where; OD_C: represents the control optical density, and OD_T: refers to the test optical density

2.8. Degradation of *E. coli* biofilm by mannan

The method employed by Wu *et al*., (2019b) was carried out with slight modifications to investigate the degradation impact of mannan on *E. coli* biofilm. Initially, 96-wells of a flat-bottom plate were inoculated individually with 180 µl of Brain heart infusion broth containing 2 % sucrose and 20 µl of a bacterial suspension equivalent to a density of 0.5 MacFarland. The plate was then incubated at 37 °C for 72 h. After gentle removal of their contents, each well was supplemented with the mannan suspension at the MIC, and the microtiter plate was subsequently incubated again at 37 °C for 24 h. After incubation, 200 µl of a 0.1 % crystal violet solution was added to each well, and then allowed to react for 20 min. before being washed with a saline solution. Afterwards, 200 ml of 95 % ethanol was added to each well, and the optical density was measured at 630 nm using an ELISA reader. The control wells were filled with 200 µl of dist. H_2O, and two replicates were used. The percentage (%) of biofilm degradation was calculated using Equation (3).

2.9. Statistical analysis

Statistical tests were performed to analyze, summarize, and present the data. The analysis of variance (ANOVA) was used to describe the percentage representation of the isolates. All analyses were performed using Microsoft® EXCEL software.

3. Results

3.1. The most productive baker's yeast sample of crude mannan and its deproteinization

Mannan was extracted from all the five baker's yeast samples, and the productivity of each sample was evaluated to determine the most efficient yeast isolate. The yield (%) representing the efficiency of mannan extraction; protein concentration, and the carbohydrate content for each sample are provided in Table (1). Among the five tested yeast samples, sample 2 of *S. cerevisiae* exhibited the highest productivity of crude mannan. The crude mannan obtained from *S. cerevisiae* 2 undergone a deproteinization step to selectively remove the naturally occurring proteins associated with *S. cerevisiae*. This deproteinization method displayed a high removal rate of about 99.6 %. The various stages of protein removal during the mannan extraction steps are detailed in Table (2).

3.2. Analysis and characterization of the purified mannan extracted and yielded from the selected *S. cerevisiae* 2

Characterization of the extracted mannan extracted from *S. cerevisiae* 2 was studied to gain a deeper understanding of its properties; structure, and behavior. By analysis and characterization of mannan, important information about its chemical composition; molecular weight, structural features, and functional properties can be obtained. This information is crucial

Table 1: The dry weight and productivity of crude mannan extracted from each sample of the baker's yeast (*S. cerevisiae*)

S. cerevisiae baker's samples*	Mannan dry wt. (g)	Yield %	Protein (mg/ ml)	Carbohydrate%
S. cerevisiae (1)	1.85[a]	37.0[a]	1.15[a]	20[a]
S. cerevisiae (2)	1.88[a]	37.6[a]	2.60[b]	40[b]
S. cerevisiae (3)	1.50[b]	30.0[b]	2.13[c]	20[a]
S. cerevisiae (4)	1.65[ab]	33.0[ab]	1.38[a]	20[a]
S. cerevisiae (5)	1.80[a]	36.0[a]	1.74[a]	20[a]

*Where; the total weight of each baker's yeast sample was 5 g. Results are averages of two replicates. Values with different superscript letters indicate significant differences among the groups at $p < 0.05$

Table 2: Deproteinization stages of the crude mannan extracted from *S. cerevisiae* 2

Stage	Total protein concentration (mg/ ml)	Deproteinization (%)
Crude mannan	2.6	0
Treatment TCA 1/ for 24 h	1.88	27.7
Treatment with three volumes of ethanol	0.14	94.6
After incubation for 3 h at 121°C	0.01	99.6

for determining and assessing the purity and quality of the extracted mannan, ensuring its suitability for the specific aims of this study.

1. Physical appearance

The purified mannan extract from *S. cerevisiae* 2 had a shiny crystalline appearance with a brown to pale yellow color. It had a smooth texture when ground with a mortar, as depicted in Fig. (1). Mannan powder had a homogeneous brown color but it didn't have a distinctive smell. Additionally, it had the ability to be easily volatilized in air.

Fig. 1: Purified mannan powder extracted from *S. cerevisiae* 2

2. Fourier transform infrared spectroscopy (FT-IR) analysis

The FT-IR analysis was performed to determine the functional groups and chemical bonds present in the purified mannan extracted from *S. cerevisiae* 2; providing insights into its molecular structure and composition. The FT-IR spectral results for detecting the functional groups of mannan are shown in Fig. (2). Several vibration zones were recorded in 3287 and 3218 cm^{-1} corresponding to the large numbers of the hydroxyl group (-OH) stretching on the sugar ring. While the vibrations in the region of 2921-2930 cm^{-1} was attributed to presence of the (C-H) group. Vibration in the range of 1645 cm^{-1} refers to the carbonyl group (C-O). The vibrations at the wavelengths of 1408, 1023, and 1198 cm^{-1} represent each of the effective functional groups resulting from O-H, C-H, and C-O-C bonds, respectively. The absorbance bond at a vibration wavelength of 972 cm^{-1} simply refers to the fingerprint region of the typical bonds in the carbohydrates, while the absorbance at a vibration of 911 cm^{-1} is typical for the α-dominating configuration in the pyranose ring of mannan. Finally, the vibration at 809 cm^{-1} refers to α-mannosidic mannan chain.

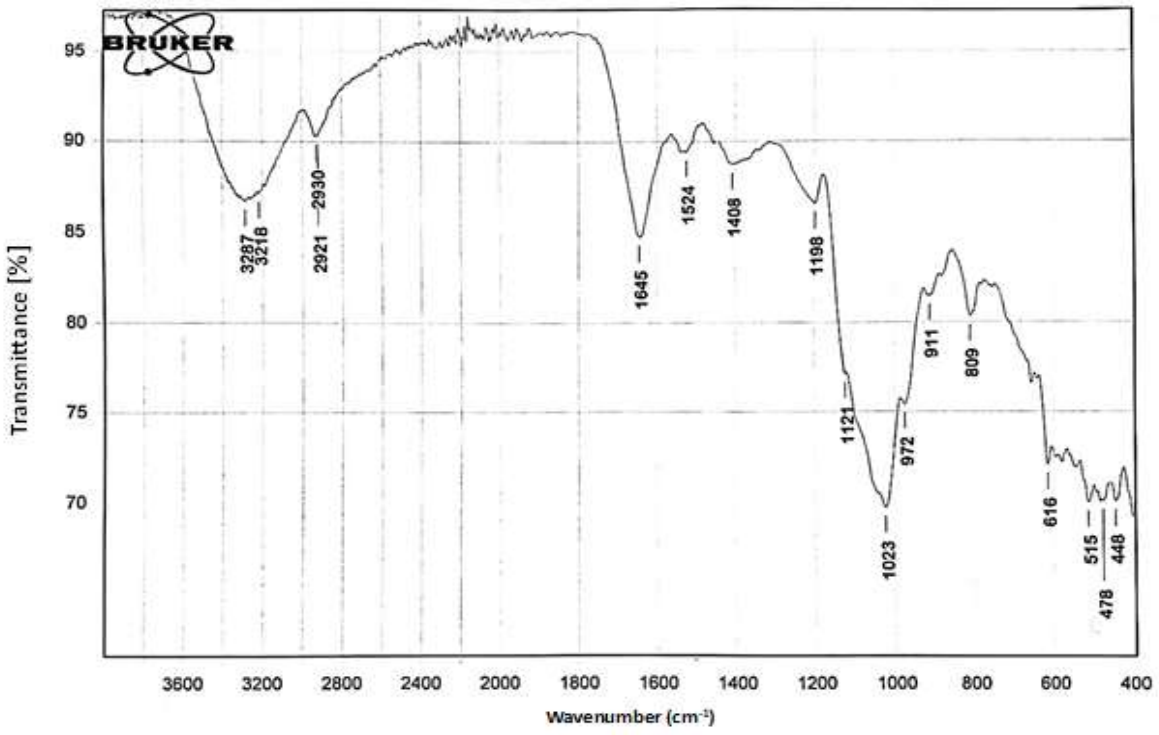

Fig. 2: FT-IR spectrum results for the purified mannan extracted from *S. cerevisiae* 2

3. Field emission scanning electron microscope (FE-SEM)

In this study, the FE-SEM technique was used to examine and explore the topography and composition of the purified mannan surface that was extracted from *S. cerevisiae* 2. The cross-sectional FE-SEM results are shown in Fig. 3(a-d). Fig. (3a) exhibits a rugged surface composed of fragmented agglomerations of varying sizes and shapes, displaying a rough and uneven texture with irregular formations. Fig. 3(b, c) showcase rough surfaces with numerous caverns and fissures; contributing to the overall uneven and rough appearance of mannan. These cracks display diverse patterns and add complexity to the bumpy surface. On the other hand, Fig. 3(d) captured at a 20 K magnification demonstrates the distinctive features of the mannan sample, appearing flat; compact, and possessing a relatively dense structure. The rough surface of mannan exhibits noticeable irregularities and texture. Notably, the image reveals the presence of multiple pores dispersed across the mannan surface, ranging in diameter from 50.24 to 106.1 nm. These pores confer a porous quality to the mannan, suggesting its capacity for absorption or exchange of liquids and gases within its structure.

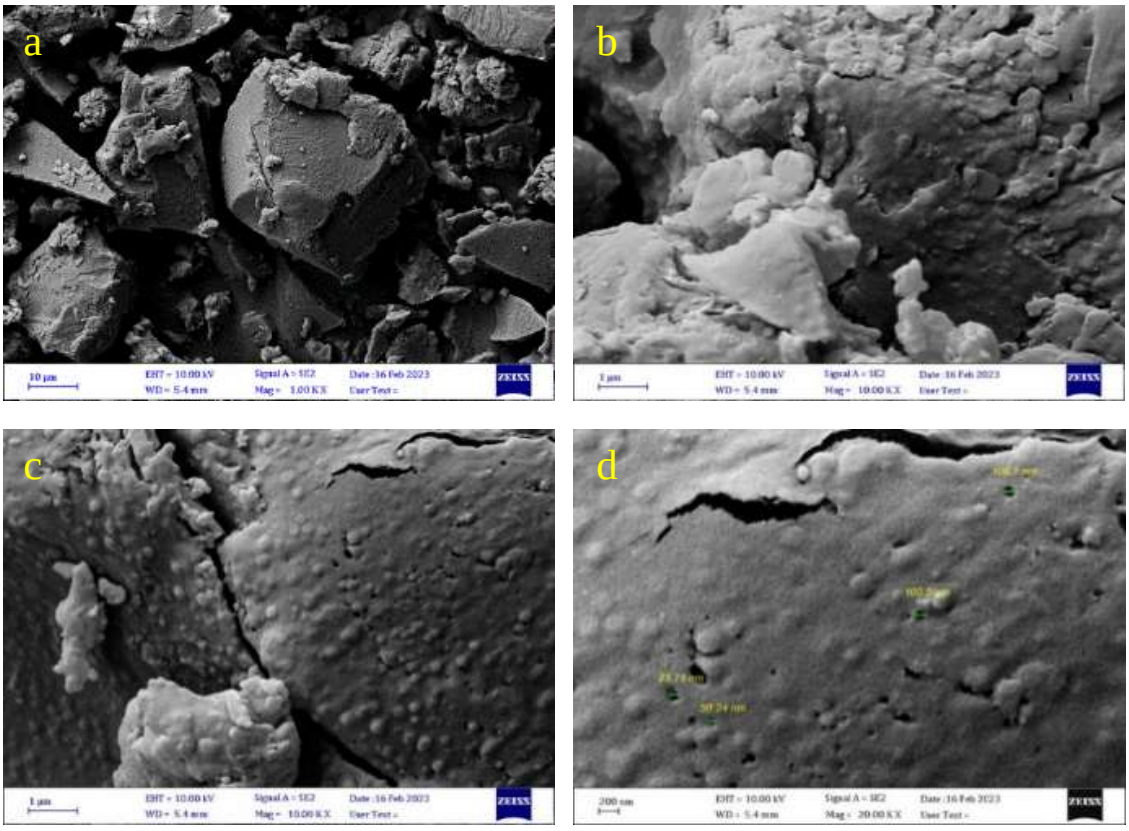

Fig. 3: FE-SEM results of the pure mannan extracted from *S. cerevisiae* 2; (a): 1 K magnification, (b): 10 K magnification, (c): 10 K magnification, and (d): 20 K magnification

4. Carbohydrates content of the purified mannan

The results of the phenol sulfuric acid method for carbohydrate content estimation revealed a concentration of 0.08 mg/ ml in the biopolymer mannan; corresponding to a total carbohydrate content of 80 %.

5. Solubility test and melting point analysis for the purified mannan

In the solubility test, the purified mannan exhibited complete solubility, where 0.1 g of the finely ground mannan powder dissolved completely within 1 min. in 10 ml of water; leaving no residual particles or agglomerates. This result indicates that it has an excellent solubility in water. Regarding the melting point analysis, the melting point of mannan was measured before and after purification using a melting point apparatus. The results showed that the melting points were 180.2 °C and 248 °C, for the crude and purified mannan, respectively.

3.3. Antimicrobial susceptibility and biofilm formation assays for identifying *E. coli* isolates

In this study, all the 112 *E. coli* isolates from the various sources were 100 % sensitive to imipenem. Additionally, 98 % and 72 % of the isolates exhibited susceptibility to Amikacin and gentamicin, while 1 % and 24 % displayed resistance to Amikacin and Gentamicin, respectively. High resistance rates were observed for Cefotaxime (75 %), with 25 % of the isolates showing sensitivity to this antibiotic. For ceftriaxone, 72 % of *E. coli* isolates were resistant and 23 % were sensitive; with 3 % exhibiting intermediate susceptibility. *E. coli* showed similar susceptibility patterns to Ciprofloxacin (59 %) and Norfloxacin (66 %), recording 35 % and 33 % resistance rates, respectively. Regarding Trimethoprim-sulfamethoxazole, 51 % exhibited susceptibility, 46 % showed resistance, and 2 % displayed intermediate susceptibility. Concerning Tetracycline; *E. coli* isolates showed a sensitivity rate of 63 %, resistance of 23 %, and 12 % intermediate susceptibility. Fig. (4) depicts the AST (%) results for *E. coli* isolates (n = 112). On the other hand, biofilm formation is a characteristic behavior of the bacterial cells where they tend to aggregate and form communities. The biofilm forming *E. coli* isolates were categorized into four groups; mainly no biofilm forming (n= 33, 29 %), weak biofilm (n= 63, 56 %), moderate biofilm (n=13, 12 %), and high biofilm forming isolates (n=3, 3 %).

3.4. Minimum inhibitory concentration of mannan against MDR-*E. coli*

This study detected MIC values of the water-soluble mannan's antibacterial effectiveness by employing a resazurin-based assay. Testing of mannan against the MDR and biofilm forming *E. coli* isolates revealed potent antibacterial activity; recording MIC values ranging from 50-100 mg/ ml, except against a single *E. coli* isolate that recorded 12.5 mg/ ml.

3.5. Antibiofilm effect of the purified mannan against MDR-*E. coli* isolates

The inhibitory efficacy assay of mannan was performed on the previously identified *E. coli* isolates that exhibited high to moderate biofilm formation; selecting three isolates from each clinical source. The results demonstrated that mannan effectively inhibited biofilm formation across all the tested MDR-*E. coli* isolates after 24 h of incubation, compared with the control group. The highest inhibition percentage for biofilm formation was observed in MDR-*E. coli* (C2) recording 37.50 %, followed by MDR-*E. coli* (U8) at 34.81 %. Conversely, the lowest inhibition percentage of 10.75 % was recorded for MDR-*E. coli* (S10), as shown in Table (3). The degradation results revealed that mannan has the ability to break down the biofilm formed by *E. coli* to varying extents. As indicated in Table (3), the highest degradation (%) was detected for the biofilm formed by MDR-*E. coli* (U8) recording 37.43 %, followed by 34.96 % for MDR-*E. coli* (S12). Conversely, mannan exhibited the lowest efficacy on degrading the biofilm formed by MDR-*E. coli* (S10).

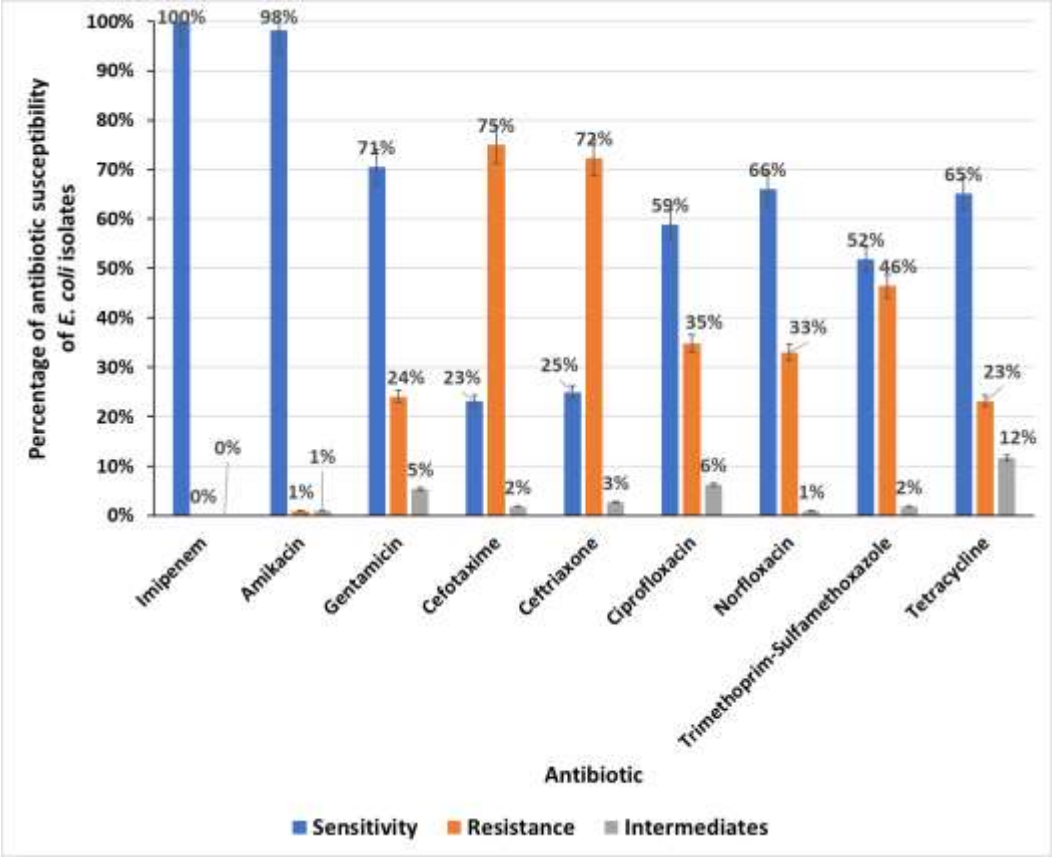

Fig. 4: Percentages (%) of antibiotic susceptibility of 112 *E. coli* isolates to 9 tested antibiotics. Results are averages of two replicates

Table 3: Antibiofilm and degradation effects of crude mannan against MDR-*E. coli*

Selected biofilm forming *E. coli* isolates	Inhibition of biofilm formation			Degradation of biofilm		
	OD_T (630 nm)	OD_C (630 nm)	%	OD_T (630 nm)	OD_C (630 nm)	%
***E. coli* (C1)**	0.127^{a}	0.167^{b}	23.95^{a}	0.134^{a}	0.152^{b}	11.84^{b}
***E. coli* (C2)**	0.095^{b}	0.152^{b}	37.50^{a}	0.202^{a}	0.223^{b}	9.41^{c}
***E. coli* (C3)**	0.039^{c}	0.044^{c}	11.36^{b}	0.123^{b}	0.164^{c}	25.0^{a}
***E. coli* (W4)**	0.060^{b}	0.078^{b}	23.08^{a}	0.394^{c}	0.413^{c}	4.60^{d}
***E. coli* (W5)**	0.119^{a}	0.135^{a}	11.85^{b}	0.131^{c}	0.135^{c}	2.96^{d}
***E. coli* (W6)**	0.118^{a}	0.093^{c}	-26.88^{d}	0.198^{c}	0.234^{c}	15.74^{b}
***E. coli* (U7)**	0.130^{a}	0.150^{b}	13.33^{b}	0.264^{c}	0.277^{c}	4.69^{d}
***E. coli* (U8)**	0.088^{c}	0.135^{b}	34.81^{a}	0.224^{c}	0.358^{d}	37.43^{a}
***E. coli* (U9)**	0.117^{a}	0.143^{b}	18.18^{a}	0.211^{c}	0.262^{d}	19.46^{a}
***E. coli* (S10)**	0.083^{c}	0.093^{c}	10.75^{b}	0.132^{c}	0.136^{c}	2.94^{d}
***E. coli* (S11)**	0.096^{b}	0.114^{b}	15.79^{a}	0.307^{d}	0.445^{e}	31.01^{a}
***E. coli* (S12)**	0.098^{b}	0.141^{b}	30.50^{a}	0.173^{d}	0.266^{d}	34.96^{a}

Where; C= MDR-*E. coli* isolated from catheter, W= isolated from wound, U= isolated from urine, S= isolated from stool, The (-) result indicates no inhibitory effect. Results are averages of two replicates. Values with different superscript letters indicate significant differences among the groups at $p < 0.05$

4. Discussion

The yeast wall primarily consists of carbohydrates, which account for approximately 85-90 % of its composition, while proteins make up the remaining 10-15 % (Harbah, 2021). To extract mannan from the baker's yeast wall, it is important to release the associated proteins into the aqueous medium. This was achieved currently through a series of extraction phases, including the use of a suitable solvent like NaOH; repeated centrifugation, and precipitation with cold ethanol, which aimed at effectively separating the protein from mannan. Optimal removal of protein attached to mannan was accomplished by heating the mixture at 121 °C under low pH conditions.

Ethanol was employed during the precipitation process, resulting in the gradual separation of multipolar polysaccharides. The use of ethanol lowers the dielectric constant of the polysaccharides, allowing for the removal of lower molecular weight sugar components, due to their enhanced compatibility with alcohol. This process leads to fragmentation of the polysaccharide molecule into different sub-fractions (Fu *et al*., 2023). Washing the precipitate with diethyl ether and absolute ethanol, along with centrifugation to eliminate the insoluble particles, further purified the baker's yeast sample and prevented hindrance of the extraction process at the various stages.

Deproteinization is a crucial step in mannan extraction as it removes the unwanted proteins from the mannan oligosaccharide (MOS) samples, resulting in a highly purified form of the oligosaccharide. The TCA method was employed for this purpose; particularly for samples containing protein content below 25 mg/ ml. This method reduces the pH 3, leading to disruption of the hydrogen bonds that exist between the proteins and the attached polymers, resulting in protein precipitation (Du et al., 2020; Thomas *et al*., 2022). Direct UV measurement of the protein provided a faster and easier alternative to colorimetry for protein quantification. However, it is important to note that this method is susceptible to interference from the other substances such as DNA, which absorbs light at a wavelength of 260 nm. Direct UV measurement allows for a relative assessment of protein sample contamination with nucleic acids (Oliveira *et al*., 2022). The protein spectrum exhibits a highly sensitive region around 280 nm; including mannan from *S. cerevisiae*, which contained residual glucose continuously bound to the proteins in both of the yeast cell wall and the periplasmic space (Liu *et al*., 2018).

The appearance characteristics of mannan, including color; purity, consistency, odor, and general powder appearance, were studied to evaluate its quality and distinguish it from the other products in the market. These characteristics allow the consumers to choose the mannan product that best suits their needs and preferences. In the various fields, such as the food industry, the specific appearance characteristics of mannan powder, including color; consistency, and solubility in liquids and other ingredients, play significant roles in its selection and application (Qui, 2023).

Currently, the spectrum analysis of the mannan sample by FT-IR confirmed that the purified saccharide was indeed mannan, and revealed the presence of glycosidic bonds α (1-6) and α (1-2). The α (1-6) linkage is the main connection bond in the mannan molecule, typically accounting for over 50 % of the total connections. The presence of hydroxyl groups served as a distinctive indicator for the carbohydrates, where the polysaccharide contained a significant number of hydroxyl groups, in accordance with Karaca *et al*., (2022); Magengelele *et al*., (2023). Furthermore, the carbonyl group in mannan enabled its potential bonding with the other compounds such as nickel carbonyl; through the metal carbonyl bonds (Kuligowski *et al*., 2012), indicating the mannan potential applications in several fields, such as vaccine production and medical device coatings. The polar

nature of the carbonyl group influenced the physical properties of the entire mannan molecule, in agreement with Zhang *et al*., (2022); Khan *et al*., (2023).

FE-SEM analysis of mannan revealed important surface traits. The tiny holes or cracks in the mannan polymer could result in filtration or absorption of the other substances, leading to interactions with the environmental materials or absorption of the liquid materials, which could affect the physical and mechanical properties of this polymer. The size of the surface pores in mannan correlated with the intermolecular or intramolecular forces, while the rough surface and perforations could affect the overall appearance and texture of the polymer; potentially causing surface imperfections, in consistence with Najeeb *et al*., (2021). These properties caused the development of porous carbon materials that are derived from the biomass-based carbohydrates, such as mannan, thus becoming highly attractive for applications in the organic synthesis, offering tunable properties; excellent catalytic activity, and stability (Lin *et al*., 2022).

Solubility of mannan in water is of a great importance due to its predominant functions in the water-based environments. Water-soluble polymers, including mannan, have significant potentials in the various industries and applications. They could be utilized to create thin films or orally dissolvable tablets, facilitating rapid and efficient drug absorption into the body (Letinski *et al*., 2021). Moreover, the water-soluble polymers have several applications as stabilizers and dispersants in the food and beverage industry, enhancing consistency; texture, and stability of the food products. The dissolution rate of mannan could be influenced by its particle size, as smaller mannan particles lead to a larger surface area that is exposed to water, and consequently resulting in faster dissolution. Additionally, higher solubility is expected in vehicles with a greater amorphous content (Faustino *et al*., 2023).

The melting point of mannan is an important parameter that influences its applications and usage. It serves as an indicator of the quality of the product, in addition to several other factors such as particle size; shape, and strength of the intermolecular bonds. The melting point of mannan is typically determined at a standard pressure of 1 atmosphere or 100 kilopascals, providing valuable insights into its characteristics (Iyer *et al*., 2023).

Mannan polymer consists of the main sugar unit D-Mannose, which represents the primary point of attachment to *FemH* located at the tip of the fimbriae. Fimbriae are small and hair-like structures used by the bacteria for attachment and biofilm growth (Scribano *et al*., 2020). A previous study conducted by Rodrigues and Elimelech, (2009) explored the impact of D-Mannose concentration on biofilm production by *E. coli* K12 wild type and pSH2 plasmid-carrying strains. They revealed that a 1% D-Mannose concentration resulted in optimal biofilm density in the microtiter plates; however, biofilm formation decreased when the D-Mannose concentration was raised to 5 %. This study also emphasized the role of gene expression on biofilm formation; specifically for the genes associated with type 1 Fimbriae protein in *E. coli*. The ability of *E. coli* to recognize D-Mannose as the principal component of mannan is crucial in reducing bacterial adhesion to the solid surfaces, thereby inhibiting biofilm formation (Wu *et al*., 2019a). In addition to inhibiting the ability of bacteria to form biofilms, biofilm degradation represents a second strategy for eliminating the bacterial biofilms. However, Wille and Coenye, (2020) revealed that a biofilm-dispersing agent must be combined with the antimicrobial agent to more effectively eliminate this costly phenomenon in terms of health and finances. Biofilm degradation occurs by attacking the biofilm matrix, which leads to the decomposition and disruption of its components, as the biofilm matrix represents a protective support for the microbial community within it (Flemming and Wingender, 2010). Variation in the ability of mannan to break down the biofilms is attributed to several reasons

related to the bacterial strain; in terms of its age and the genes responsible for polysaccharide formation, which constitutes the largest component of the biofilm matrix. The polysaccharides present in the matrix are interconnected through glycosidic bonds (Rabin *et al*., 2015).

Conclusion

Extraction of mannan from the baker's yeast cell involved multiple phases to separate the proteins from carbohydrates, utilizing several techniques, including solvents; centrifugation, precipitation, and purification. Optimizing these processes is crucial for obtaining a highly purified mannan for the various applications. Mannan has been found to inhibit the formation of MDR-*E. coli* biofilms by creating physical barriers that hinder bacterial adhesion. Additionally, degradation of a biofilm by mannan has been investigated as a strategy to disrupt the existing *E. coli* biofilms, thus weakening their structure and promoting the bacterial cell dispersal.

Acknowledgements

The authors would like to acknowledge the staff in the laboratories of the College of Science at Mustansiriyah University, Baghdad, Iraq (www.uomustansiriyah.edu.iq) for their support during the current work.

Conflict of interests

The authors declare no conflicts of interest.

Funding source

This study was self-funded by the authors. Some laboratory equipment and materials in the laboratories of the College of Science at Mustansiriyah University were used in this research after obtaining the required approvals.

Ethical approval

The Mustansirihya University, College of Science, Ethical Committee approval code is BCSMU/1221/00017M. Written consents of the participants were provided.

Author's Contributions

Conceptualization, N.A. and J.S.; Data curation, N.A. and J.S.; Investigation, N.A. and P.S.; Supervision, J.S.; Validation, N.A. and J.S.; Roles/Writing - original draft, N.A.; Writing - review & editing, N.A. and J.S.

5. References

Abdulhameed, E.H.; Sattar Salman, J.A. and Majeed, H.Z. (2020). Production, characterization, and antibacterial effects of dextran from *Saccharomyces cerevisiae* strains obtained from different commercial products available in the Iraq market. International Journal of Pharmaceutical Research. 12(2): 2836-2844. https://doi.org/10.31838/ijpr/2020.SP2.173

Al-Manhel, A. and Niamah, A. (2017). Mannan extract from *Saccharomyces cerevisiae* used as prebiotic in bio-yogurt production from buffalo milk. International Food Research Journal. 24(5): 2259-2264. http://www.ifrj.upm.edu.my/24%20(05)%202017/(58).pdf

Ballash, G.A.; Mollenkopf, D.F.; Diaz-Campos, D.; van Balen, J.C.; Cianciolo, R.E. and Wittum, T.E. (2022). Pathogenomics and clinical recurrence influence biofilm capacity of *Escherichia coli* isolated from canine urinary tract infections. PloS one. 17(8): 1-16. https://doi.org/10.1371/journal.pone.0270461

Ballén, V.; Cepas, V.; Ratia, C.; Gabasa, Y. and Soto, S.M. (2022). Clinical Escherichia coli: From Biofilm Formation to New Antibiofilm Strategies. Microorganisms. 10(6): 1103. https://doi.org/10.3390/microorganisms10061103

Brenner, D.J.; Krieg, N.R.; Staley, J.T. and Garrity, G. (2005). Bergey's Manual® of Systematic

Bacteriology: Volume Two: The Proteobacteria (Part C), Springer. https://doi.org/10.1007/0-387-29298-5

Cerqueira, M.A.; Souza, B.W.; Simões, J.; Teixeira, J.A.; Domingues, M.R.M.; Coimbra, M.A. et al. (2011). Structural and thermal characterization of galactomannans from non-conventional sources. Carbohydrate Polymers. 83(1): 179-185. https://doi.org/10.1016/j.carbpol.2010.07.036

Dash, S.; Vashisht, N.; Sinha, S.; Kumar, A. and Goyal, K. (2023). Forensic implication of seized drug imitating methamphetamine with mileage in crime. Egyptian Journal of Forensic Sciences. 13(1): 1-6. https://doi.org/10.1186/s41935-023-00325-6

Du, L.; Arauzo, P.J.; Meza Zavala, M.F.; Cao, Z.; Olszewski, M.P. and Kruse, A. (2020). Towards the properties of different biomass-derived proteins *via* various extraction methods. Molecules. 25(3): 488. https://doi.org/10.3390/molecules25030488

DuBois, M.; Gilles, K.A.; Hamilton, J.K.; Rebers, P.T. and Smith, F. (1956). Colorimetric method for determination of sugars and related substances. Analytical Chemistry. 28(3): 350-356. https://doi.org/10.1021/ac60111a017

Elsayed, A.; Safwat, A.; Abdelsattar, A.S.; Essam, K.; Nofal, R.; Makky, S. et al. (2023). The antibacterial and biofilm inhibition activity of encapsulated silver nanoparticles in emulsions and its synergistic effect with *E. coli* bacteriophage. Inorganic and Nano-Metal Chemistry. 53(6): 549-559. https://doi.org/10.1080/24701556.2022.2081191

Faustino, M.; Pereira, C.F.; Durão, J.; Oliveira, A.S.; Pereira, J.O.; Ferreira, C. et al. (2023). Effect of drying technology in *Saccharomyces cerevisiae* mannans: Structural, physicochemical, and functional properties. Food chemistry. 412: 135545. https://doi.org/10.1016/j.foodchem.2023.135545

Flemming, H.C. and Wingender, J. (2010). The biofilm matrix. Nature Reviews Microbiology. 8(9): 623-633. https://doi.org/10.1038/nrmicro2415

Fu, M.; Mi, S.; Zhao, J.; Wang, X.; Gao, J. and Sang, Y. (2023). The interaction mechanism, conformational changes and computational simulation of the interaction between surface layer protein and mannan at different pH levels. Food chemistry. 405: 135021. https://doi.org/10.1016/j.foodchem.2022.135021

Gil, D.; Zarzycka, M. and Laidler, P. (2023). Mechanics of Cells and Tissues in Diseases. In: Lekka, M.; Navajas, D.; Radmacher, M. and Podestà, A. (Editors). Volume 2 Biomedical Applications. 23-33. https://doi.org/10.1515/9783110989380-003

Haney, E.F. and Hancock, R.E.W. (2022). Addressing Antibiotic Failure-Beyond Genetically Encoded Antimicrobial Resistance. Frontiers in Drug Discovery. 2: 892975. https://doi.org/10.3389/fddsv.2022.892975

Haney, E.F.; Trimble, M.J. and Hancock, R.E. (2021). Microtiter plate assays to assess antibiofilm activity against bacteria. Nature Protocols. 16(5): 2615-2632. https://doi.org/10.1038/s41596-021-00515-3

Harbah, R.; Meledina, T.V.; Manshin, D.V. and Andreev, V.V. (2021). Mannan: structure, biosynthesis, and methods extraction from yeast *Saccharomyces cerevisiae*. Journal of International Academy of Refrigeration. 1: 59-65. https://doi.org/10.17586/1606-4313-2021-20-1-59-65

Huang, G.L. (2008). Extraction of two active polysaccharides from the yeast cell wall. Z Naturforsch C Journal of Biosciences. 63(11-12): 919-921. https://doi.org/10.1515/znc-2008-11-1224

Huang, G.; Yang, Q. and Wang, Z.B. (2010). Extraction and deproteinization of mannan oligosaccharides. Z Naturforsch C Journal of

Biosciences. 65(5-6): 387-390. https://doi.org/10.1515/znc-2010-5-611

Iyer, J.; Brunsteiner, M.; Modhave, D. and Paudel, A. (2023). Role of Crystal disorder and Mechanoactivation in Solid-state Stability of Pharmaceuticals. Journal of Pharmaceutical Sciences. 112(6): 1539-1565. https://doi.org/10.1016/j.xphs.2023.02.019

Karaca, B.; Haliscelik, O.; Gursoy, M.; Kiran, F.; Loimaranta, V.; Söderling, E. et al. (2022). Analysis of Chemical Structure and Antibiofilm Properties of Exopolysaccharides from *Lactiplantibacillus plantarum* EIR/IF-1 Postbiotics. Microorganisms. 10(11): 2200. https://doi.org/10.3390/microorganisms10112200

Khan, H.; Faizan, M.; Niazi, S.U.K.; Madiha; Muhammad, N. and Zhang, W. (2023). Water-Soluble Carbon Monoxide-Releasing Molecules (CORMs). Topics in Current Chemistry. 381(1): 3. https://doi.org/10.1007/s41061-022-00413-6

Kuligowski, J.; Quintás, G.; Herwig, C. and Lendl, B. (2012). A rapid method for the differentiation of yeast cells grown under carbon and nitrogen-limited conditions by means of partial least squares discriminant analysis employing infrared micro-spectroscopic data of entire yeast cells. Talanta. 99(20-10): 566-573. https://doi.org/10.1016/j.talanta.2012.06.036

Kunz Coyne, A.J.; El Ghali, A.; Holger, D.; Rebold, N. and Rybak, M.J. (2022). Therapeutic strategies for emerging multidrug-resistant *Pseudomonas aeruginosa*. Infectious Diseases and Therapy. 11(2): 661-682. https://doi.org/10.1007/s40121-022-00591-2

Laconi, A.; Tolosi, R.; Apostolakos, I. and Piccirillo, A. (2023). Biofilm Formation Ability of ESBL/*pAmpC*-Producing *Escherichia coli* Isolated from the Broiler Production Pyramid. Antibiotics. 12(1): 155. https://doi.org/10.3390/antibiotics12010155

Letinski, D.J.; Redman, A.D.; Birch, H. and Mayer, P. (2021). Inter-laboratory comparison of water solubility methods applied to difficult-to-test substances. BMC Chemistry. 15(1): 52. https://doi.org/10.1186/s13065-021-00778-7

Lin, Y.; Yu, J.; Zhang, X.; Fang, J.; Lu, G.-P. and Huang, H. (2022). Carbohydrate-derived porous carbon materials: An ideal platform for green organic synthesis. Chinese Chemical Letters. 33(1): 186-196. https://doi.org/10.1016/j.cclet.2021.06.045

Liu, Y.; Huang, G. and Lv, M. (2018). Extraction, characterization and antioxidant activities of mannan from yeast cell wall. International Journal of Biological Macromolecules. 118(Part A): 952-956. https://doi.org/10.1016/j.ijbiomac.2018.06.145

Loo, Y.Y.; Rukayadi, Y; Nor-Khaizura, M.A.R.; Kuan, C.H.; Chieng, B.W.; Nishibuchi, M. et al. (2018). *In Vitro* Antimicrobial Activity of Green Synthesized Silver Nanoparticles Against Selected Gram-negative Foodborne Pathogens. Frontiers in Microbiology. 9: 1555. https://doi.org/10.3389/fmicb.2018.01555

Magengelele, M.; Malgas, S. and Pletschke, B.I. (2023). Bioconversion of spent coffee grounds to prebiotic mannooligosaccharides-an example of biocatalysis in biorefinery. RSC Advances. 13(6): 3773-3780. https://doi.org/10.1039/D2RA07605E

Najeeb, M.I.; Hameed Sultan, M.T.; Md Shah, A.U.; Muhammad Amir, S.M.; Safri, S.N.A.; Jawaid, M. et al. (2021). Low-velocity impact analysis of pineapple leaf fiber (PALF) hybrid composites. Polymers. 13(18): 3194. https://doi.org/10.3390/polym13183194

Oliveira, A.S.; Ferreira, C.; Pereira, J.O.; Pintado, M.E. and Carvalho, A.P. (2022). Spent brewer's yeast (*Saccharomyces cerevisiae*) as a potential source of bioactive peptides: An overview. International Journal of Biological Macromolecules. 208: 1116-1126. https://doi.org/10.1016/j.ijbiomac.2022.03.094

Qui, N.H. (2023). Baker's Yeast (*Saccharomyces cerevisiae*) and its application on poultry's production and health: A review. Iraqi Journal of Veterinary Sciences. 37(1): 213-221. https://doi.org/10.33899/ijvs.2022.132912.2146

Rabin, N.; Zheng, Y.; Opoku-Temeng, C.; Du, Y.; Bonsu, E. and Sintim, H.O. (2015). Biofilm formation mechanisms and targets for developing antibiofilm agents. Future Medicinal Chemistry. 7(4): 493-512. https://doi.org/10.4155/fmc.15.6

Reis, S.F.; Messias, S.; Bastos, R.; Martins, V.J.; Correia, V.G.; Pinheiro, B.A. et al. (2023). Structural differences on cell wall polysaccharides of brewer's spent *Saccharomyces* and microarray binding profiles with immune receptors. Carbohydrate Polymers. 301: 120325. https://doi.org/10.1016/j.carbpol.2022.120325

Rodrigues, D.F. and Elimelech, M. (2009). Role of type 1 fimbriae and mannose in the development of *Escherichia coli* K12 biofilm: from initial cell adhesion to biofilm formation. Biofouling. 25(5): 401-411. https://doi.org/10.1080/08927010902833443

Salam, M.A.; Al-Amin, M.Y.; Salam, M.T.; Pawar, J.S.; Akhter, N.; Rabaan, A.A. et al. (2023). Antimicrobial Resistance: A Growing Serious Threat for Global Public Health. Healthcare. 11(13): 1-20. https://doi.org/10.3390/healthcare11131946

Scribano, D.; Sarshar, M.; Prezioso, C.; Lucarelli, M.; Angeloni, A.; Zagaglia, C. et al. (2020). D-Mannose treatment neither affects uropathogenic *Escherichia coli* properties nor induces stable *FimH* modifications. Molecules. 25(2): 316. https://doi.org/10.3390/molecules25020316

Sonola, V.S.; Katakweba, A.; Misinzo, G. and Matee, M.I. (2022). Molecular Epidemiology of Antibiotic Resistance Genes and Virulence Factors in Multidrug-Resistant *Escherichia coli* Isolated from Rodents, Humans, Chicken, and Household Soils in Karatu, Northern Tanzania. International Journal of Environmental Research and Public Health. 19(9): 5388. https://doi.org/10.3390/ijerph19095388

Thomas, A.; Gasch, B.; Olivieri, E. and Quintard, A. (2022). Trichloroacetic acid fueled practical amine purifications. Beilstein Journal of Organic Chemistry. 18(1): 225-231. https://doi.org/10.3762/bjoc.18.26

Tong, Y.C.; Zhang, Y.N.; Li, P.C.; Cao, Y.L.; Ding, D.Z.; Yang, Y. et al. (2023). Detection of antibiotic-resistant canine origin *Escherichia coli* and the synergistic effect of magnolol in reducing the resistance of multidrug-resistant *Escherichia coli*. Frontiers in Veterinary Science. 10: 1104812. https://doi.org/10.3389/fvets.2023.1104812

Topa, S.H.; Subramoni, S.; Palombo, E.A.; Kingshott, P.; Rice, S.A. and Blackall, L.L. (2018). Cinnamaldehyde disrupts biofilm formation and swarming motility of *Pseudomonas aeruginosa*. Microbiology. 164(9): 1087-1097. https://doi.org/10.1099/mic.0.000692

Wille, J. and Coenye, T. (2020). Biofilm dispersion: The key to biofilm eradication or opening Pandora's box? Biofilm. 2: 100027. https://doi.org/10.1016/j.bioflm.2020.100027

Wu, H.; Zhang, W. and Mu, W. (2019a). Recent studies on the biological production of D-mannose. Applied Microbiology and Biotechnology. 103: 8753-8761. https://doi.org/10.1007/s00253-019-10151-3

Wu, Y.; Wang, R.; Xu, M.; Liu, Y.; Zhu, X.; Qiu, J. et al. (2019b). A novel polysaccharide depolymerase encoded by the phage SH-KP152226 confers specific activity against multidrug-resistant *Klebsiella pneumoniae via* biofilm degradation. Frontiers in Microbiology. 10: 2768. https://doi.org/10.3389/fmicb.2019.02768

Yousefi, L. (2023). Yeast Mannan: Structure, Extraction and Bioactivity. Applied Food Biotechnology. 10(3): 155-164. https://doi.org/10.22037/afb.v10i3.41489

Zhang, D.; Zheng, Y.; Yuan, G.; Qian, G.; Zhang, H.; You, Z. et al. (2022). Chemical characteristics analyze of SBS-modified bitumen containing composite nanomaterials after aging by FTIR and GPC. Construction and Building Materials. 324: 126522. https://doi.org/10.1016/j.conbuildmat.2022.126522

Zhao, Y.; Wang, J.; Fu, Q.; Zhang, H.; Liang, J.; Xue, W. et al. (2022). Characterization and Antioxidant Activity of Mannans from *Saccharomyces cerevisiae* with Different Molecular Weight. Molecules. 27(14): 4439. https://doi.org/10.3390/molecules27144439

Zimmer, J.; Bonertz, A.; Kaul, S. and Vieths, S. (2022). Introduction of General Chapters on standard methods for allergen quantification in the European Pharmacopoeia. Allergy. 78(4): 895-1126. https://doi.org/10.1111/all.15631